Cell Reports, Volume *41*

Supplemental information

Dissecting the genetic and microenvironmental factors of gastric tumorigenesis in mice

Zhenghao Lu, Ailing Zhong, Hongyu Liu, Mengsha Zhang, Xuelan Chen, Xiangyu Pan, Manli Wang, Xintong Deng, Limin Gao, Linyong Zhao, Jian Wang, Yi Yang, Qi Zhang, Baohong Wu, Jianan Zheng, Yigao Wang, Xiaohai Song, Kai Liu, Weihan Zhang, Xiaolong Chen, Kun Yang, Xinzu Chen, YingLan Zhao, Chengjian Zhao, Yuan Wang, Lu Chen, Zongguang Zhou, Jiankun Hu, Yu Liu, and Chong Chen

SUPPLEMENTARY INFORMATION

This file includes:

Tables S1 to Tables S5

All supplementary tables of this study can be found in Microsoft Excel documents.

Supplementary Figure 1 to Supplementary Figure 6

Supplementary Figure 1

Supplementary Figure 2

Supplementary Figure 3

Supplementary Figure 4

Supplementary Figure 5

Supplementary Figure 6

Supplementary Figure 1

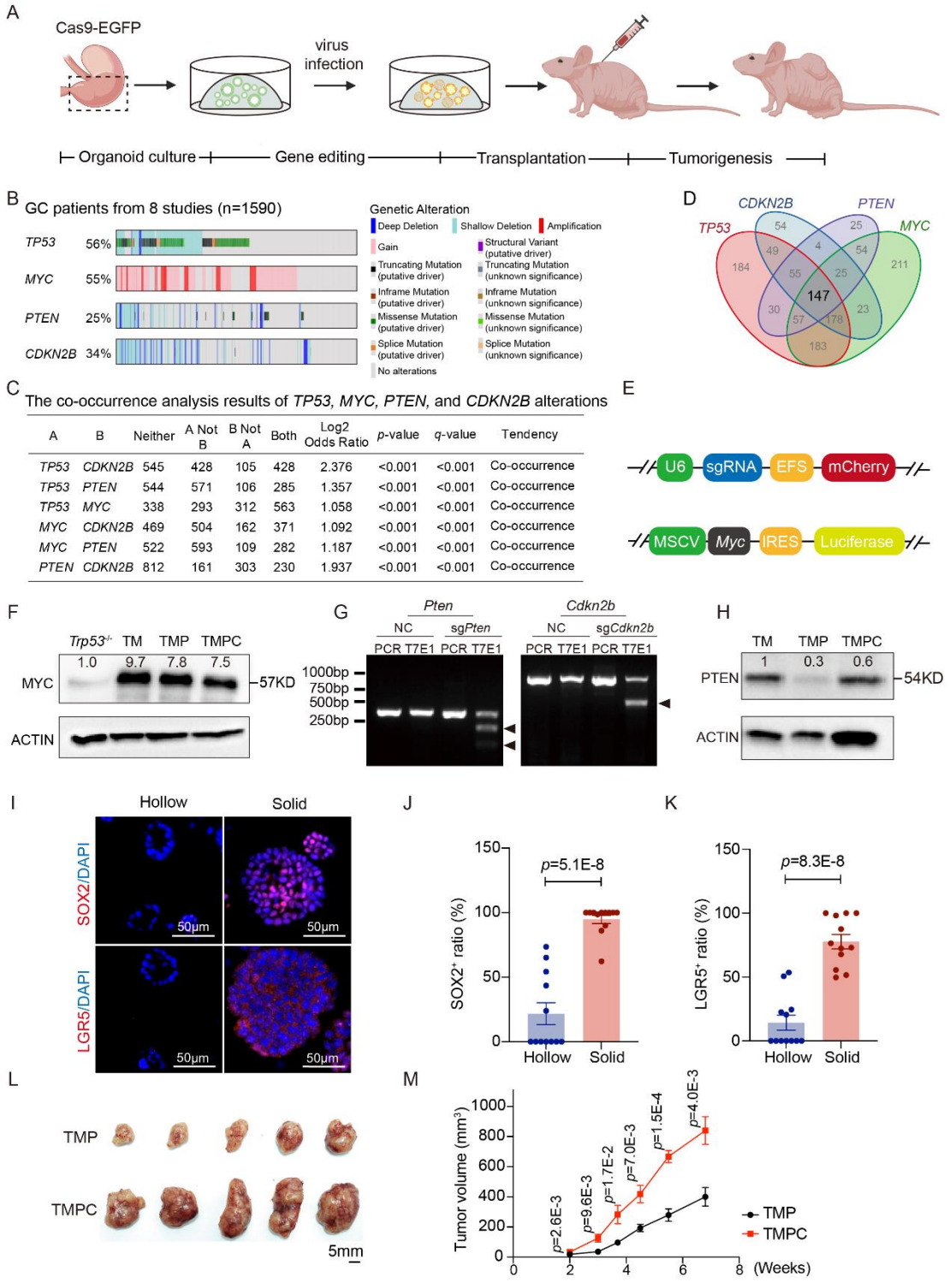

Figure S1. Generating and charactering primary dysplasia, well-differentiated and poorly differentiated adenocarcinoma from engineered organoids in mice, related to Figure 1.

(A) Schematic diagram of the strategy for generating subcutaneous mouse model with CRISPR/Cas9-edited stomach organoids.

(B) The OncoPrint showing the variation frequencies of *TP53*, *MYC*, *PTEN* and *CDKN2B* in 1590 gastric cancer samples from 8 studies.

(C) The co-occurrence of *TP53*, *MYC*, *PTEN* and *CDKN2B* variations in gastric cancer patients. Data were analyzed from cBioPortal public datasets. The significance levels of co-occurrence were calculated by the statistical method Mutual Exclusivity Modules, provided by the cBioPortal.

(D) The Venn diagram showing 147 patients harbored all *TP53*, *MYC*, *PTEN* and *CDKN2B* alterations.

(E) Schematic of the constructs for expressing sgRNAs (top) and *Myc* (bottom).

(F) Western blotting showing the protein levels of MYC in *Trp53*$^{-/-}$, TM, TMP and TMPC organoids.

(G) T7 endonuclease I assay on *Pten* (left) or *Cdkn2b* (right) in TMPC organoids. Cleaved bands were pointed by arrowheads, NC indicates the negative control.

(H) Western blotting showing the protein levels of PTEN in TM, TMP and TMPC organoids.

(I) Representative immunofluorescent staining of SOX2 and LGR5 in hollow and solid organoids. Scale bar, 50μm.

(J) The ratio of SOX2^{+} cells in hollow and solid organoids (n=12). Data presented as the means ± the SEM, *p*-value was calculated by unpaired *t*-test.

(K) The ratio of LGR5^{+} cells in hollow and solid organoids (n=12). Data presented as the means ± the SEM, *p*-value was calculated by unpaired *t*-test.

(L) The bright field images of subcutaneous TMP and TMPC tumors (n = 5).

(M) The growth curves of subcutaneous TMP and TMPC tumors (n = 5). Data presented as the means ± the SEM, *p*-value was calculated by unpaired *t*-test.

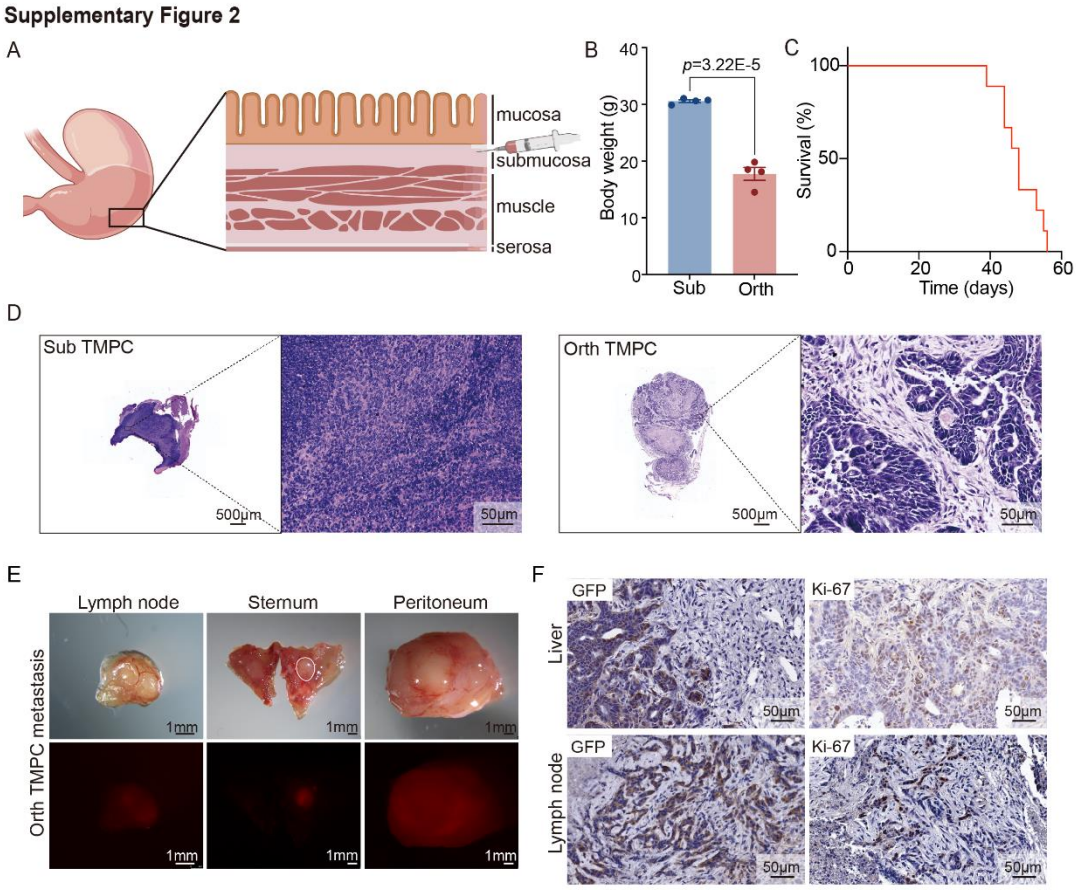

Figure S2. Orthotopically transplanted TMPC organoids give rise to metastatic carcinomas, related to Figure 2.

(A) Schematic for orthotopically transplanted TMPC organoids.

(B) The body weight of sacrificed subcutaneous and orthotopic TMPC mice (n = 4). Data presented as the means ± the SEM, *p*-value was calculated by unpaired *t*-test.

(C) Survival curve of orthotopically transplanted TMPC mice (n = 9).

(D) Representative H&E images of lymph nodes of subcutaneous (left) and orthotopic(right) TMPC mice. Scale bar, 500μm (left) and 50μm (right).

(E) Representative bright-field (top) and red fluorescence (bottom) images of lymph node (left), sternum (middle) and peritoneum (right) metastases from the orthotopic TMPC mice. Scale bar, 1mm.

(F) Representative GFP (left) and Ki-67 (right) staining of liver (top) and lymph node (bottom) metastases in orthotopic TMPC mice. Scale bar, 50μm.

Supplementary Figure 3

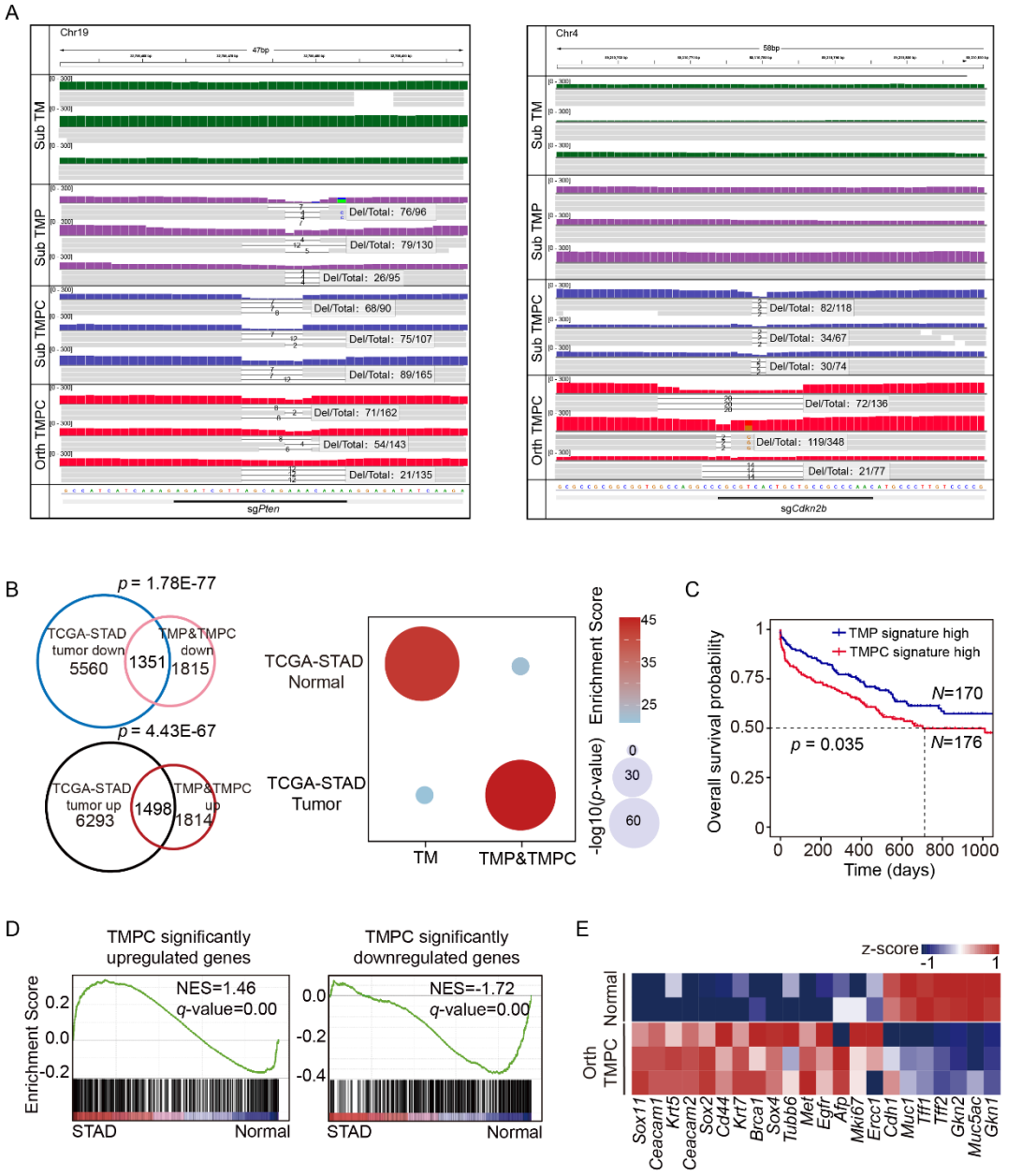

Figure S3. The molecular features of the subcutaneous and orthotopic GCs, related to Figure 3.

(A) Integrative Genomics Viewer exhibiting the editing sites and efficiency of sg*Pten* (left) and sg*Cdkn2b* (right) in subcutaneous TM, TMP, TMPC tumors and orthotopic TMPC tumors (n = 3).

(B) The Venn diagrams showing overlapping of the down or up regulated genes in patients' tumors compared to adjacent normal tissues with TMP&TMPC down or up regulated genes compared to TM groups, respectively (left). The dot plot

showing the enrichment scores of TM, TMP&TMPC mouse tumor tissues, human normal and tumor tissues. GC patient data were analyzed from the TCGA-STAD cohorts. Statistic values were determined by hypergeometric test.

(C) The Kaplan-Meier survival curves of patients with high expression levels of TMP and TMPC signature genes in the TCGA-STAD cohort. Statistical significance was determined by Log-rank test.

(D) GSEA showing the similarity of gene expression patterns between mouse models and GC patients. Compared to mouse normal tissues, TMPC up-regulated genes significantly enriched in human tumors and TMPC down-regulated genes significantly enriched in tumor-adjacent normal tissues.

(E) The heatmap showing the expression levels of marker genes of gastric normal epithelial and adenocarcinoma between normal tissues and TMPC orthotopic tumors.

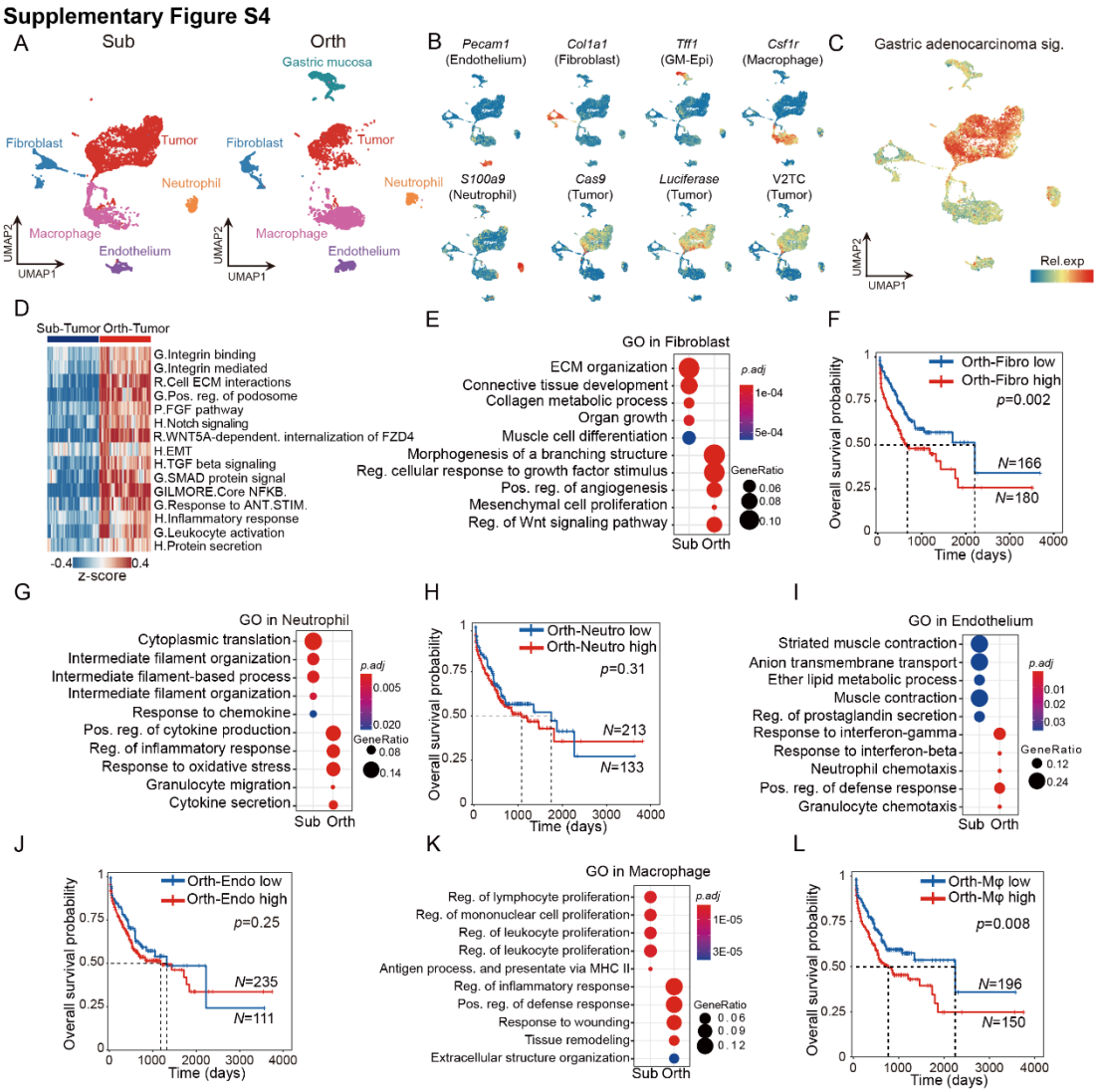

Figure S4. Single cell transcriptome analyses reveal the cellular and molecular differences between the subcutaneous and orthotopic TMPC tumors, related to Figure 4.

(A) The UMAP plots showing sample origins from subcutaneous and orthotopic tumors (subcutaneous cells = 6825, orthotopic cells = 5426).

(B) The expression levels of eight representative marker genes in each cell type.

(C) The UMAP plot showing the expression levels of human GC signature in each cell type.

(D) The heatmap showing the positively enriched pathways of orthotopic tumor cells, compared to subcutaneous tumor cells (G: GO, H: Hallmark, R: Reactome).

(E) The GO enrichment results of subcutaneous and orthotopic fibroblasts.

(F) The Kaplan-Meier survival curves of TCGA-STAD patients with low and high expression levels of orthotopic fibroblast signature genes. Statistical significance was determined by Log-rank test.

(G) The GO enrichment results of subcutaneous and orthotopic neutrophils.

(H) The Kaplan-Meier survival curves of TCGA-STAD patients with low and high expression levels of orthotopic neutrophil signature genes. Statistical significance was determined by Log-rank test.

(I) The GO enrichment results of subcutaneous and orthotopic endothelium.

(J) The Kaplan-Meier survival curves of TCGA-STAD patients with low and high expression levels of orthotopic endothelium signature genes. Statistical significance was determined by Log-rank test.

(K) The GO enrichment results of subcutaneous and orthotopic macrophages.

(L) The Kaplan-Meier survival curves of TCGA-STAD patients with low and high expression levels of orthotopic macrophage signature genes. Statistical significance was determined by Log-rank test.

Supplementary Figure 5

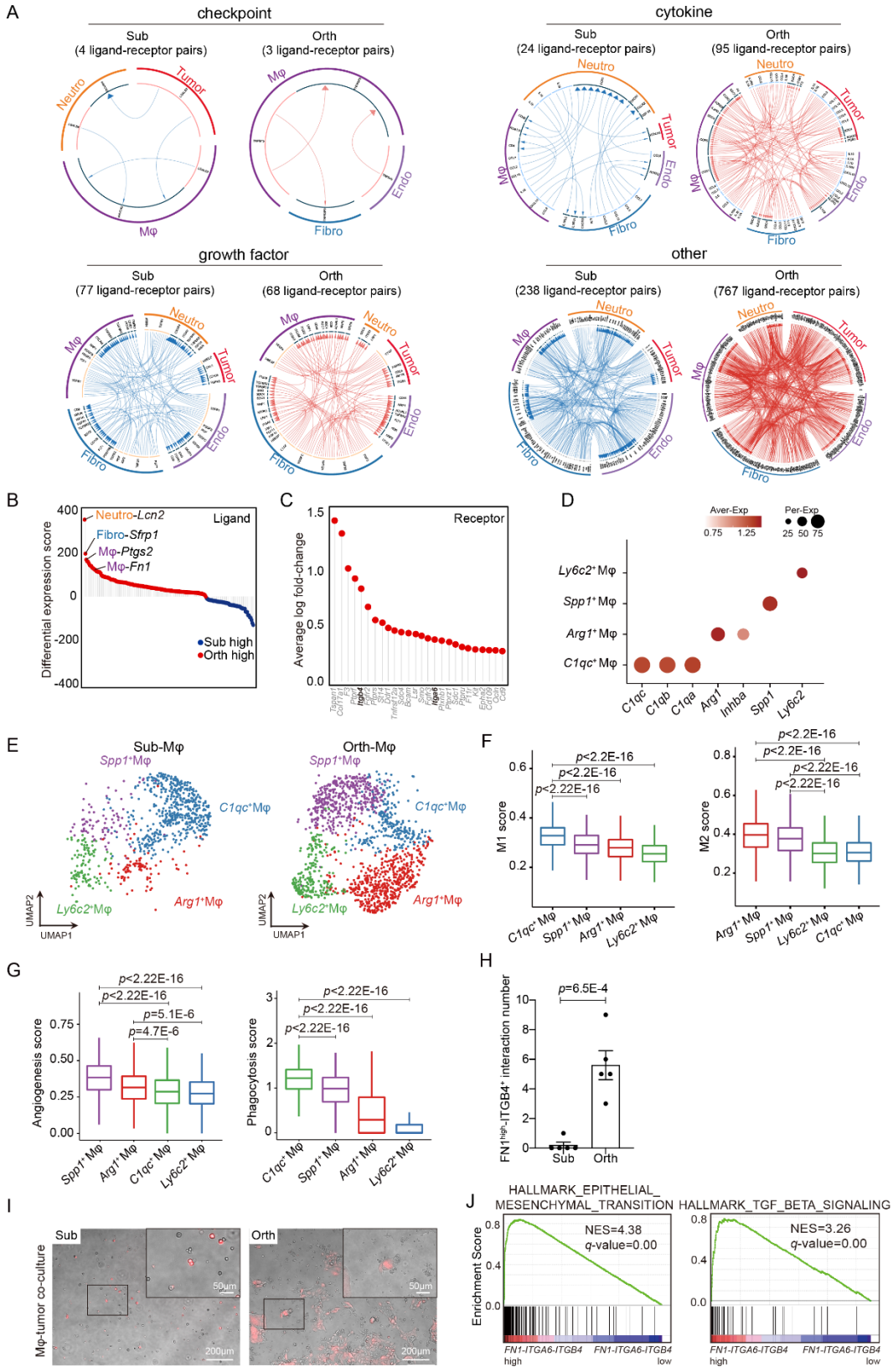

Figure S5. FN1^{high} macrophages interact with tumor cells through integrin α6β4,

related to Figure 5.

(A) Network plots showing the differential expression ligand-receptor interaction pairs between subcutaneous and orthotopic tumors.

(B) The lollipop plot showing 200 differentially expressed ligand genes between subcutaneous and orthotopic non-tumor cells.

(C) The lollipop plot showing 26 receptor genes significantly highly expressed in tumor cells, compared to non-tumor cell populations. Average $\log_2$ fold change > 0.25, *p-adj* < 0.05, two-tailed Wilcoxon's rank-sum tests based on Bonferroni correction.

(D) The dot plot showing the expression levels of marker genes for each macrophage subpopulation.

(E) The UMAP plots showing four subpopulations in subcutaneous (left) and orthotopic (right) macrophages.

(F) The expression levels of M1(left) and M2 (right) signature genes in four macrophage subpopulations. Two-tailed Wilcoxon's rank-sum tests were used to determine the significance levels.

(G) The expression levels of the angiogenesis (left) and phagocytosis (right) signature genes in four macrophage subpopulations. Two-tailed Wilcoxon's rank-sum tests were used to determine the significance levels.

(H) The interaction number of $FN1^{high}$ macrophages and $ITGB4^{+}$ tumor cells (n = 5). Data presented as the means ± the SEM, *p*-value was calculated by unpaired *t*-test.

(I) Representative images of macrophages adhering to the subcutaneous and orthotopic TMPC tumor cells (red). Scale bar, 200μm. Box areas showing higher magnifications. Scale bar, 50μm.

(J) GSEA showing the enrichments of HALLMARK_EPITHELIAL_MESEN-CHYMAL_TRANSITION and HALLMARK_TGF_BETA_SIGNALING pathways in GC patients with high *FN1-ITGA6-ITGB4* expression levels compared to those with low.

Supplementary Figure 6

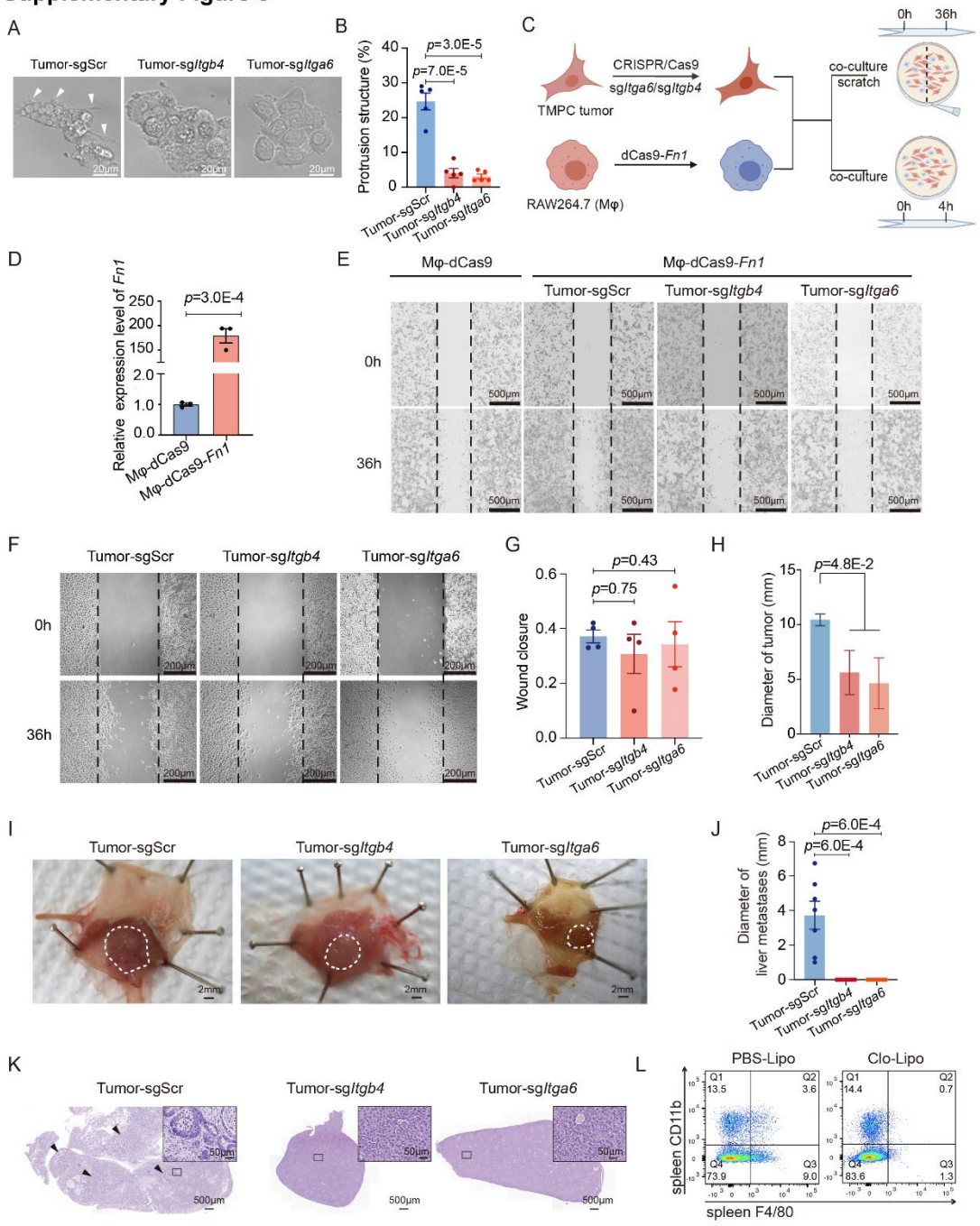

Figure S6. FN1^{high} macrophages promote liver metastasis of GC via integrin α6β4 in vitro and in vivo, related to Figure 6.

(A) Representative images showing the morphologies of orthotopic TMPC tumor cells with sgScr, sg*Itgb4* and sg*Itga6* in 2D culture. Scale bar, 20μm.

(B) The percentage of protrusion structures in TMPC tumor cells with sgScr, sg*Itgb4* or sg*Itga6* (n = 5). Data presented as the means ± the SEM, *p*-value was calculated by unpaired *t*-test.

(C) Flow chart of the scratch-wounding cell migration and the adhesion assay.

(D) Relative expression levels of *Fn1* in Mφ-dCas9 and Mφ-dCas9-*Fn1*, measured by qPCR. Data presented as the means ± the SEM, *p*-value was calculated by unpaired *t*-test.

(E) Representative scratch-wounding images of the TMPC tumor cells with sgScr, sg*Itgb4* or sg*Itga6* were co-cultured with Mφ-dCas9 or Mφ-dCas9-*Fn1*. Scale bar, 500μm.

(F) Representative scratch-wounding images of the TMPC tumor cells with sgScr, sg*Itgb4* or sg*Itga6*. Scale bar, 200μm.

(G) The bar plot showing the wound closure score in TMPC tumor cells with sgScr, sg*Itgb4* or sg*Itga6* (n = 4), measured by Image J. Data presented as the means ± the SEM, *p*-value was calculated by unpaired *t*-test.

(H) The bar plot showing the diameter of orthotopic TMPC tumors with sgScr, sg*Itgb4*, or sg*Itga6*. Data presented as the means ± the SEM, *p*-value was calculated by unpaired *t*-test.

(I) Representative bright-field images of orthotopic TMPC tumors with sgScr, sg*Itgb4* or sg*Itga6*. Circled areas indicate tumor region. Scale bar, 2mm.

(J) The bar plot showing the diameter of metastasis loci in the liver of orthotopic TMPC with sgScr, sg*Itgb4* or sg*Itga6* recipient mice (n = 7). Data presented as the means ± the SEM, *p*-value was calculated by unpaired *t*-test.

(K) Representative H&E staining of the liver section of orthotopic TMPC with sgScr, sg*Itgb4* or sg*Itga6* recipient mice. Arrowheads indicate the metastases loci. Scale bar, 500μm. Box areas showing higher magnifications. Scale bar, 50μm.

(L) Representative flow cytometric profiles of F4/80 macrophages in the spleen of mice injected with PBS-Lipo or Clo-Lipo from orthotopic TMPC mice.